Synchrotron radiation interferometry for beam size measurement at low current and in large dynamic range

Wei Li,* Jun Yan, Peifan Liu, and Ying K. Wu†

FEL Laboratory, TUNL and Department of Physics, Duke University, Durham, North Carolina 27708-0319, USA

(Received 17 May 2022; accepted 4 August 2022; published 17 August 2022)

The Synchrotron Radiation Interferometry (SRI) has become a widely used technique to measure the small transverse size of the electron beam in the storage ring. In a typical SRI system for the routine storage ring operation, synchrotron radiation from a dipole magnet is used to illuminate a double slit with a small slit opening and a relatively large slit separation to form a large number of interference fringes on the observation plane. However, a different type of SRI is needed for intrabeam scattering (IBS) research to measure the beam size at ultralow currents and in a wide dynamic range. Such a system requires a double slit with a large slit opening to increase the light input while having the capability of accurately measuring the beam size with a range of visibility. By examining the impact of the nonuniform wave amplitude of synchrotron radiation and that of the varying visibility (due to a changing beam size) on the beam size measurement, we propose a new physics model for this type of SRI. This new model is validated using simulation, showing significantly improved results when compared with the conventional model. Based on this new model, we have developed and tested an SRI system dedicated to the IBS study on the Duke storage ring. This system has been used successfully to measure electron beams with about 10 μA of current and with a higher current but a variable size. This new physics model can also improve the measurement accuracy and consistency of the conventional SRIs, especially at low visibility.

DOI: 10.1103/PhysRevAccelBeams.25.080702

I. INTRODUCTION

The transverse beam emittance is a crucial parameter for the performance of a storage ring-based synchrotron radiation light source and charged particle collider. The commonly used method to determine the beam emittance in the storage ring is to measure the transverse beam size and beta function at a particular location. Due to its nondestructive nature, synchrotron radiation is often used to measure the beam size in electron storage rings. A widely used technique to measure the transverse beam profile is based on the direct imaging method. Several different imaging techniques have been developed with the system's resolution limited by the diffraction effect [1]. To increase the resolution, the measurement system can be operated in a short wavelength, such as VUV or x ray. With a Fresnel zone plate or a pinhole camera, an image resolution of a few μm can be achieved [2,3]. However, such a system is difficult to setup as it requires an in-vacuum operation and either expensive VUV optics such as the zone plate or a lot of space for a pine-hole system [3–6]. Furthermore, due to the lack of high energy radiation at a low-energy storage ring, the image-based system is limited to operate in the visible to UV region with relatively poor resolution of tens of μm [7–10].

To achieve a high resolution, a beam size measurement technique based on the interferometric method has been developed to explore the spatial coherence of synchrotron radiation in the visible or UV spectrum [11,12]. In such a synchrotron radiation interferometry (SRI), a quasimonochromatic light beam prepared using a narrow-band filter illuminates a double slit and the emerging wavefronts are focused onto the image plane to form interference fringes. The modulation depth of the fringes (the visibility) is measured to determine the size of an electron beam in the Gaussian distribution. Conventionally, the SRI has been developed to measure a small vertical beam size with a reasonable large visibility. This usually leads to the use of a double slit with two narrow slits and a relatively wide slit separation. The typical interference pattern from such an SRI is shown in Fig. 1(a) with a large number of interference fringes inside the main diffraction envelope. This type of SRI is suitable for the routine storage ring operation with a sufficiently large beam current and a relatively small beam size variation.

*wl227@duke.edu
†wu@phy.duke.edu

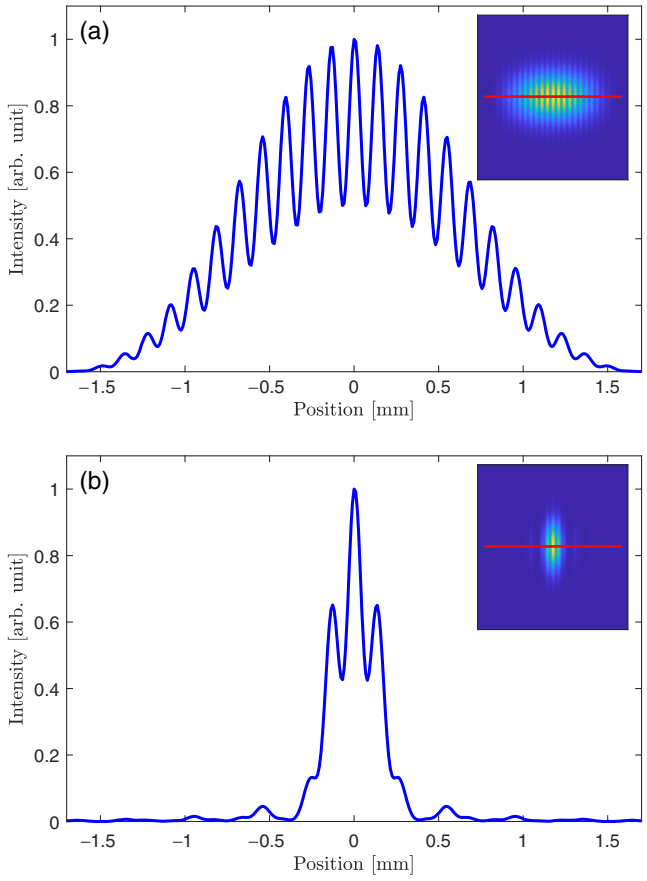

FIG. 1. Illustration of interference patterns simulated using the Synchrotron Radiation Workshop (SRW) with two different double slits. (a) Simulated for a conventional SRI measurement system with a large number of interference fringes inside the main diffraction envelope. The slit separation is 5 mm and the slit opening is 0.4 mm. (b) Simulated for an SRI system with a large slit opening and a relatively small slit separation: only a few interference fringes are present inside the main diffraction envelope. The slit separation is 5 mm and the slit opening is 1.8 mm. For each subplot, the inset shows the image of the interference fringes. In each subplot, the projection of the simulated intensity distribution is shown with the data from a red rectangle in the inserted image. The x axis is scaled to be equal in both plots.

For the study of beam dynamics in the storage ring such as the intrabeam scattering (IBS) effect, the beam size measurements need to be conducted for a wide range of the beam current, including very low currents. To increase the light illumination on the image detector (e.g., a digital camera), the slit opening needs to be enlarged. As a result, the number of interference fringes will be significantly reduced, as shown in Fig. 1(b). In addition, for the IBS study, the SRI should be developed with a large dynamic range to measure the changing beam size in a wide range due to the beam current change and for a range of electron beam energies. However, the current physics model for the SRI has been developed with two important assumptions: (1) synchrotron radiation on the double slit can be approximated as a spherical wave with a uniform amplitude; and (2) the beam size is very small so that the diffraction envelope does not change with the beam size. For a dedicated SRI system developed for the IBS study, both assumptions are problematic. To overcome these shortcomings of the existing model, we have developed a new and more general physics model for the SRI which can account for the features of the nonuniform distributed incident synchrotron radiation beam and a wide range of operating parameters. In the following context, this model will be referred to as the "new model" or "new fitting model."

This work is motivated by our IBS research to be conducted on the Duke storage ring. This storage ring is well suited for such research because of its wide range of operation parameters, from 250 to 1.2 GeV and a few μA to 100 mA in a single-bunch beam. This requires us to develop a dedicated SRI to accurately measure the small vertical size of the beam at a very low current and in a wide range. To accomplish this, we need to develop a new type of SRI and the related physics model to enable its operation in a much broader range of parameters.

In this paper, we will first review the physics principle and assumptions made to model the conventional SRI system in Sec. II. In Sec. III, we first discuss the impact of the nonuniform intensity distribution of synchrotron radiation and the impact of the beam size on the measurements. We then develop new ideas to mitigate these adverse effects and propose a new model for the SRI. In Sec. IV, the new model is validated and compared with the old or standard model using simulation. Section V presents the preliminary experimental results of a newly developed SRI system used to measure the vertical beam size in the Duke storage ring in two different cases: (1) at a low beam current of about 10 μA and (2) at a varying vertical beam size by changing the emittance coupling. The work is summarized in Sec. VI, followed by discussions on how this new model can be used to improve the measurement accuracy and consistency of the conventional SRI systems and how it may be explored for the measurement of a single-pass beam.

II. REVISIT OF SRI METHOD

It is well known that in a double-slit experiment, an interference pattern can be produced using a light beam with spatial coherence. The idea of using spatial coherence to measure the size of a small incoherent radiation source stems from the van Cittert-Zernike theorem [13]. This method has been successfully utilized to measure the small transverse size of a charged particle beam at multiple accelerator facilities [11,14–17].

A typical optical system using synchrotron radiation interferometry to measure the electron beam size is shown in Fig. 2. In this setup, at a distance L_1 downstream from the electron beam, the optical wavefront is intercepted by a double slit of width d and separation D. Immediately after the slit, a thin focusing lens is placed to produce an

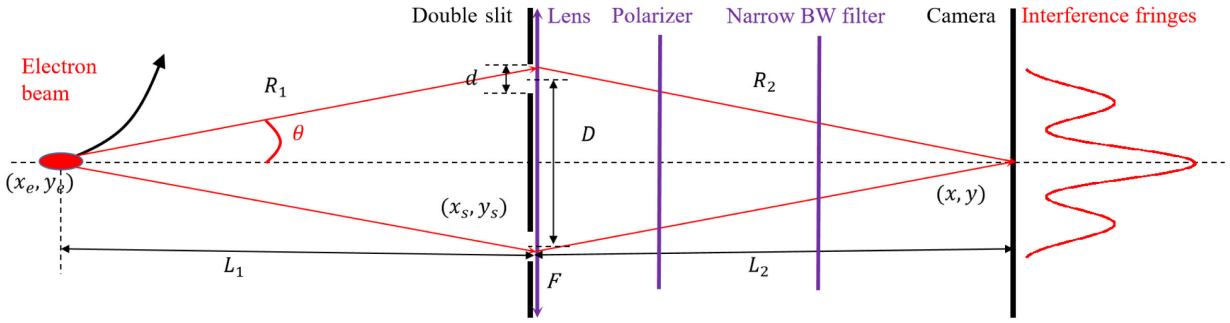

FIG. 2. Optical layout of an SRI-based electron beam size measurement system. Synchrotron radiation from the electron beam propagates through a double slit and a focusing lens, producing an interference pattern on the image plane of the lens, which is captured by a digital camera. A linear polarizer with its polarizing axis aligned horizontally and a narrow bandpass filter are used to improve the system performance.

interference pattern on the image plane. Recorded using a camera, the interference pattern is analyzed to determine the degree of the intensity modulation (the visibility), which is directly related to the electron beam size. In such an SRI measurement system, a polarization filter is used to select the beam polarization, and a narrow band-pass filter is used to produce a nearly monochromatic light beam [11].

Synchrotron radiation emitted by an electron traversing a bending magnet can be approximated using a spherical wave under certain circumstances [14]. This wavefront propagates through an aperture to form the diffraction pattern on the observation plane. This phenomenon can be described using the Rayleigh-Sommerfeld diffraction formula using a complex electric field U [13],

$$U(\vec{r}_e,\vec{r}) = \frac{1}{2\pi}\int_S \frac{Ae^{-ikR_1}}{R_1}\left(ik+\frac{1}{R_1}\right)\frac{e^{-ikR_2}}{R_2}\cos(\theta)\,dS, \qquad (1)$$

where $\vec{r}_e = (x_e, y_e)$ and $\vec{r} = (x, y)$ are the positions of the electron on the object plane and the measurement point on the observation plane, respectively, A is the wave amplitude, $k = 2\pi/\lambda$ is the wave vector, R_1 is the distance from the electron to a point on the aperture plane, R_2 is the distance from this point to the measurement point on the observation plane, and θ is the angle between the wavefront propagation direction and the normal direction of the aperture plane. The integration is carried out over the entire aperture of area S.

The above expression can be simplified using the far-field approximation, $k \gg 1/R_1$, and the paraxial approximation, $\theta \ll 1$. In the case that a thin focal lens is located at the same location as the aperture (see Fig. 2), the lens provides a phase shift to the wavefront. Under these conditions, the electrical field on the observation plane can be expressed as follows:

$$U(\vec{r}_e,\vec{r}) \approx \frac{ik}{2\pi}\int_S A\frac{e^{-ikR_1}}{R_1}\exp\left(\frac{ikr_s^2}{2f}\right)\frac{e^{-ikR_2}}{R_2}\,dS, \qquad (2)$$

where $\vec{r}_s = (x_s, y_s)$ is the position of a surface element dS on the aperture plane and f is the focal length.

The observed intensity distribution on the observation plane for a single electron is $I(\vec{r}_e,\vec{r}) \propto |U(\vec{r}_e,\vec{r})|^2$. Since radiation from electrons in the beam is incoherent, the intensity distribution for the whole beam can be calculated by integrating over the entire beam,

$$I(\vec{r}) = \int I(\vec{r}_e,\vec{r})\rho(\vec{r}_e)dV, \qquad (3)$$

where $\rho(\vec{r}_e)dV$ is the number of electrons in a small volume dV.

Let us consider the problem of measuring the vertical beam size using a horizontal double slit as the aperture (see Fig. 2). After the slit, the vertically spaced horizontal interference fringes will be formed on the image plane. The image distance (L_2) and the source distance (L_1) are related to the thin lens focal length (f):

$$\frac{1}{f} = \frac{1}{L_1} + \frac{1}{L_2}. \qquad (4)$$

In the wave phase, the distances R_1 and R_2 can be approximated by keeping the second-order terms under the Fresnel approximation, i.e., $\max|\Delta y_i|^4 \ll L_i^3\lambda$, where $\Delta y_1 = y_s - y_e$ and $\Delta y_2 = y_s - y$, then $R_i \approx L_i + (\Delta y_i)^2/(2L_i)$ with $i = 1, 2$. The electric field on the observation plane can be obtained for a single electron

$$U(y_e, y) = U_0\frac{\sin\psi(y_e,y)}{\psi(y_e,y)}\cos\left[\frac{\phi(y_e,y)}{2}\right] \qquad (5)$$

where

$$\psi(y_e, y) = \frac{\pi d}{\lambda}\left(\frac{y_e}{L_1} + \frac{y}{L_2}\right) \qquad (6)$$

and

$$\phi(y_e, y) = \frac{2\pi D_y}{\lambda}\left(\frac{y_e}{L_1} + \frac{y}{L_2}\right), \tag{7}$$

with D_y being the vertical separation of the slits. The resultant intensity distribution of the vertical interference fringes on the observation plane can be derived for a single electron

$$\frac{I(y_e, y)}{I_0} = \left[\frac{\sin\psi(y_e, y)}{\psi(y_e, y)}\right]^2 [1 + \cos\phi(y_e, y)], \tag{8}$$

where I_0 is related to the maximum intensity of the fringes. In Eq. (8), the sinc function term represents the diffraction effect of a single slit as a broad intensity envelope while the cosine function term represents the interference pattern between the two slits.

With the assumption that the vertical charge distribution is Gaussian and can be described by a normalized linear density,

$$\rho(y_e) = \frac{1}{\sqrt{2\pi}\sigma_y}\exp\left[-\frac{(y_e - y_0)^2}{2\sigma_y^2}\right], \tag{9}$$

where σ_y is the vertical beam size and y_0 is the center position of the electron beam. The intensity distribution of the interference fringes can be obtained using Eq. (3) by assuming that the diffraction envelope does not depend on the electron's position:

$$\begin{aligned}\frac{I(y)}{I_0} &= \int \left[\frac{\sin\psi(y_e, y)}{\psi(y_e, y)}\right]^2 [1 + \cos\phi(y_e, y)]\rho(y_e)dy_e \\ &\approx \left[\frac{\sin\psi_0(y)}{\psi_0(y)}\right]^2 [1 + V\cos\phi_0(y)],\end{aligned} \tag{10}$$

where $\psi_0(y) = \frac{\pi d}{\lambda}(\frac{y_0}{L_1} + \frac{y}{L_2})$ and $\phi_0(y) = \frac{2\pi D_y}{\lambda}(\frac{y_0}{L_1} + \frac{y}{L_2})$, V is known as the visibility of the interferometry which is explicitly related to the vertical beam size

$$V = \exp\left[-\frac{1}{2}\left(\frac{2\pi D_y}{\lambda L_1}\sigma_y\right)^2\right] \quad \text{or} \quad \sigma_y = \frac{\lambda L_1}{2\pi D_y}\sqrt{2\ln\frac{1}{V}}. \tag{11}$$

This is the standard model for synchrotron radiation interferometry for the beam size measurement in the literature [11,14]. However, this treatment could yield inaccurate measurement results due to two important approximations made: (1) the slit opening and beam size are small so that the slit diffraction pattern remains unchanged for all electrons in the beam, i.e., $\psi(y_e, y) \approx \psi(y_0, y)$; (2) synchrotron radiation is modeled using a spherical wave, ignoring the fact that its wave amplitude depends on the emission angle. In the following section, we will present techniques to overcome these limitations to make the SRI method applicable to a wider range of operational conditions, as well as to improve the results of the systems with conventional setups.

III. NEW MODEL FOR SRI

In the SRI, the intensity distribution of a single electron emission on the observation plane is determined by the diffraction pattern from every single slit ($F_{\text{diffraction}}$) and the interference pattern from the double slit ($G_{\text{interference}}$) [18], which can be denoted as follows:

$$\frac{I(y_e, y)}{I_0} = F_{\text{diffraction}} \otimes G_{\text{interference}}. \tag{12}$$

The "⊗" indicates that the resultant intensity distribution is the convolution of the single-slit diffraction and the interference of the diffracted beams from the two slits. The diffraction of the slit determines the envelope of the intensity distribution on the observation plane: a narrow slit opening produces a broad diffraction envelope. The interference due to the light from two slits forms the bright-dark fringes. The change of a single electron's vertical position leads to a vertical shift of the diffraction envelope, as well as the locations of the interference fringes. While derived mathematically for a simple situation with a plane wave, Eq. (12) captures the most important features of the interference fringes on the observation plane.

In this work, we will use this idea to construct a model system that can be extended to the cases of nonplane waves and with large slit openings. In this section, we will develop methods to handle the impact of the wave amplitude variation on the interference pattern as well as the impact of beam size on the diffraction pattern. Finally, we will propose a more general fitting model to reduce these impacts on the beam size measurements using the synchrotron radiation interferometry.

A. Impact of nonuniform wave amplitude

It is known that the power of synchrotron radiation emitted by an electron beam is not uniformly distributed in all directions. It has a nonuniform distribution in the vertical direction, with a decreasing amplitude as the emission angle θ is increased as shown in Fig. 3. Hence, the wave amplitude in Eq. (1) is not a constant, but a function of the emission angle θ, $A = A(\theta)$ [19].

The double slit can be treated as a series of virtual double slits with very narrow openings and their separations varying from $D_1 = D_y - d$ to $D_2 = D_y + d$. For each symmetrically arranged virtual slit pair, the incident beam intensity is the same. The intensity distribution on the observation plane is the accumulation of interference fringes from all virtual double slits. Let us consider two pairs of virtual double slits with separations D_1 and D_2, respectively, as shown in Fig. 3. In the scenario that the light intensity is uniform, two sets of virtual double slits,

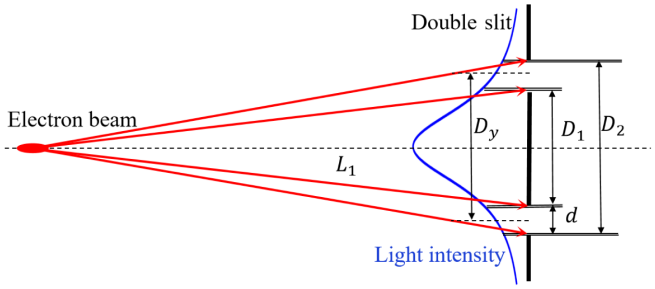

FIG. 3. Distribution of the synchrotron radiation intensity (blue curve) on the double slit, showing the nonuniformity light illumination over each single slit.

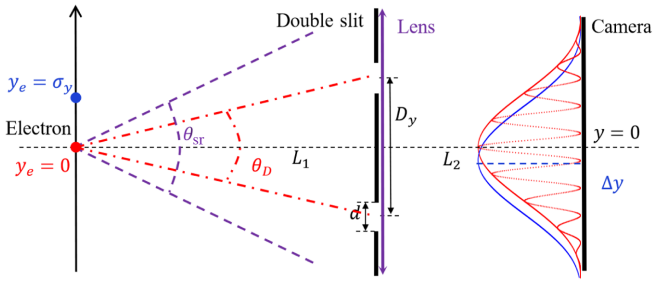

FIG. 4. Illustration of the shifting of the single-slit diffraction envelope on the image plane due to the change of the electron's vertical position. On the left side, the red dashed lines show the opening angle (θ_{sr}) of synchrotron radiation from an in-plane electron ($y_e = 0$). The purple dash-dotted lines show the angle (θ_D) subtended by the two slits. On the right side, the red and blue solid curves represent the single-slit diffraction patterns produced by an in-plane and off-plane ($y_e = \sigma_y$) electron, respectively, with the red dotted curve showing the double-slit interference pattern for the in-plane case.

D_1 and D_2, contribute equally to the intensity distribution on the observation plane. As a result, the modulation of the interference fringes is determined by the average value of two double slits, $(D_1 + D_2)/2 = D_y$, the separation between the centers of the two physical slits. The situation changes in the scenario that the light intensity is not uniform. For example, the power of synchrotron radiation reduces with the increase of the opening angle θ. In this case, the intensity is higher for the pair of the virtual slits with a smaller separation D_1 than the pair with a large separation D_2. The interference fringe will see more contribution from the virtual slit pair D_1. Consequently, the interference pattern will be associated with an effective slit separation that is smaller than the actual separation of two-slit centers, i.e., $D_y^{\text{eff}} < D_y$.

A more mathematical treatment of this effect for a linear distribution of the optical amplitude across the slit opening is given in Appendix A. The main results are summarized in the following: Let us assume that the optical amplitude on the slit plane can be expressed as $A(y_s) = a_0(1 - \alpha|y_s \mp D_y/2|)$ ("−" for the upper slit and "+" for the lower slit), with a_0 being the amplitude at the center of the slit and $-\alpha$ ($\alpha > 0$) representing the slope of the amplitude variation with respect to y_s. The analysis shows that while the intensity envelope is still determined by the slit opening d, the interference pattern is modulated by an effective slit spacing, D_y^{eff}. Integrating over the Gaussian electron beam distribution, the overall visibility is given in terms of D_y^{eff}:

$$V(D^{\text{eff}}) \approx \exp\left[-\frac{1}{2}\left(\frac{2\pi D_y^{\text{eff}}}{\lambda L_1}\sigma_y\right)^2\right], \tag{13}$$

which is the same expression as Eq. (11) if the slit spacing is given by D_y^{eff}. For this linear amplitude distribution, D_y^{eff} is given as

$$\frac{D_y^{\text{eff}}}{D_y} \approx 1 - \frac{1}{6}\frac{\alpha d^2}{D_y}. \tag{14}$$

The change of the slit separation $(D_y^{\text{eff}} - D_y)$ is proportional to $-d^2$. It becomes more significant in the cases where the slit opening d is large, i.e., the ratio d/D_y is relatively large. In our analysis, we will determine D_y^{eff} without using this linear model of the wave amplitude. The method to find D_y^{eff} directly using the measurement data will be described as part of a new fitting model below.

B. Impact of beam size on diffraction pattern

The intensity envelope is determined by the single-slit diffraction: a wide slit results in a narrow diffraction envelope. This envelope distribution is also dependent on the electron's position according to Eq. (8), i.e., the diffraction envelope from a single electron located above or below the midplane of the dipole magnet is shifted accordingly on the observation plane, as shown in Fig. 4. Integrating over the electron distribution in the vertical direction, this effect alters the diffraction envelope on the observation plane. Such a change is more pronounced for a larger beam size and a large slit with a narrower distribution.

By using a common diffraction envelope for all electrons, i.e., using $\text{sinc}^2\psi(y_e, y) \approx \text{sinc}^2\psi(y_0, y) = \text{sinc}^2\psi_0(y)$, this effect has not been taken into account in Eq. (10). By expanding $\text{sinc}^2\psi(y_e, y)$ to the first order of $(y_e - y_0)$, we can capture the main correction effect. The detailed mathematical derivation can be found in Appendix B. In the following, we summarize the main results. First, we expand the envelope term

$$\text{sinc}^2\psi(y_e, y) \approx \text{sinc}^2\psi_0(y)\left[1 - \frac{2}{3}\frac{\pi d}{\lambda L_1}\psi_0(y)(y_e - y_0)\right]. \tag{15}$$

Second, we integrate over the Gaussian electron beam distribution to yield the following intensity distribution on the observation plane:

$$\frac{I(y)}{I_0} \approx \left[\frac{\sin\psi_0(y)}{\psi_0(y)}\right]^2 \times \left\{1 + V\left[\cos\phi_0(y) + \frac{2d}{3D_y}\ln\frac{1}{V}\psi_0(y)\sin\phi_0(y)\right]\right\}. \tag{16}$$

With the above result, a few important observations can be made. First, the correction term is a sine-like term with the same fast oscillation phase $\phi_0(y)$ as the original term $\cos\phi_0(y)$, which represents a small correction of the intensity distribution with a new feature out of phase from the main term. Second, this term is proportional to $\psi_0(y)$, which means that it is small around the central diffraction region that is dominated by the original $\cos\phi_0(y)$ term; it only has important contributions toward the waist and tail regions of the diffraction intensity distribution. Third, this correction term becomes more significant for a large ratio d/D_y and for a low visibility situation with a small V. Finally, the specific coefficient in the front of $\sin\phi_0(y)$ depends on the orders of the Taylor expansion carried out, therefore, will be treated as a fitting parameter in our model.

C. Generalized fitting model

Having analyzed the impact of the large slit opening and the large beam size and developed new physics insights into ways to make corrections, we are ready to propose a more general model to better represent the interference fringes on the observation plane while keeping the model in a form consistent with the standard model, the old model, given by Eq. (10). Essentially, this new model will be a generalization of Eq. (16). Recognizing that $\psi_0(y)$ is a linear function of y, this new fitting model can be given as the following:

$$I(y) = p_0 + p_1\mathrm{sinc}^2(p_2y + p_3) \times \left(1 + e^{-p_4}\left\{\cos\left[p_5\left(y + \frac{p_3}{p_2}\right)\right] + (p_6y + p_7)\sin\left[p_5\left(y + \frac{p_3}{p_2}\right)\right]\right\}\right), \tag{17}$$

where eight parameters p_i $(i = 0, \ldots, 7)$ are used in the fitting. First, to take care of the beam size effect, the interference effect is represented by both cosine- and sine-terms with high spatial frequency, and the weight of the sine-term is given by a general linear function of y. Second, the large slit opening effect manifested as D_y^{eff} is dealt with by making the phase argument of the interference terms a fitting variable, p_5. The effective slit separation is then calculated using

$$D_y^{\mathrm{eff}} = \frac{\lambda L_2}{2\pi}p_5. \tag{18}$$

Third, the beam size is determined using the fit visibility, $V = e^{-p_4}$ and D_y^{eff} [see also Eq. (11)]

$$\sigma_y = \frac{\lambda L_1}{2\pi D_y^{\mathrm{eff}}}\sqrt{2\ln\frac{1}{V}} = \frac{L_1}{L_2p_5}\sqrt{2p_4}. \tag{19}$$

Finally, this model is further generalized to allow the fitting to determine an effective slit opening d^{eff} via fitting parameter p_2: $d^{\mathrm{eff}} = \lambda L_2 p_2/\pi$. It is worth noting that p_1 is used to represent the maximum value of the intensity distribution while p_0 is used to capture the overall background.

It is worth comparing this new model with the old fitting model based on Eq. (10):

$$I_1(y) = p_0 + p_1\,\mathrm{sinc}^2(c_1y + p_2) \times \left\{1 + e^{-p_3}\cos\left[c_2\left(y + \frac{p_2}{c_1}\right)\right]\right\}, \tag{20}$$

where p_i $(i = 0, \ldots, 3)$ are the fitting parameters and c_j $(j = 1, 2)$ are constants related to the design values of the slit opening d and slit separation D_y, respectively. In this old model, there are four fitting parameters. The most important one is p_3, determining the visibility of the interference pattern. The beam size is calculated using only one fitting parameter p_3 and the design value D_y,

$$\sigma_y = \frac{\lambda L_1}{2\pi D_y}\sqrt{2p_2}. \tag{21}$$

IV. VALIDATION OF NEW MODEL

A. Two different types of SRI systems

A conventional SRI system developed for a storage ring–based synchrotron radiation light source is used to measure the small vertical beam size for routine operation with a reasonably high beam current at a fixed electron beam energy. In this case, due to a high incident light level, a small slit opening d is chosen. The slit separation D_y is usually selected to be much larger than d to produce a large number of fringes while achieving a good visibility for the measurement of a small beam. Overall, such an SRI system typically has a narrow dynamic range.

Due to its ability to measure the small beam size, the SRI system has been considered for research in which the beam size can be varied from small to large by changing the electron beam energy and/or the beam current [20]. For example, the electron beam can be studied at a fixed energy with the beam current varied in a wide range from a few μA to 100 mA. This requires the system to have a wide dynamic range and to be capable of measuring a small transverse beam size at a low beam current. To increase the light input for the low-current measurement, a large slit opening d is chosen to increase the dynamic range while

TABLE I. Comparison of the figures of merit between conventional SRI systems and a system for beam instability studies. Case 1 is the vertical beam size measurement system at KEK-ATF [21,22] and Case 2 is the beam measurement system at BESSY-II [23]. Case 3 is the new SRI system designed for the IBS research at the Duke storage ring.

Scenario	$g_1 = \frac{D_y}{d}$	$g_2 = \frac{2\pi D_y \sigma_y}{\lambda}$
Conventional	Large	Small
IBS study	Smaller	Small–large
Case 1: KEK-ATF [21,22]	13.3	Around 0.45
Case 2: BESSY II [23][a]	3.3–8.3	0.51–1.2
Case 3: IBS Research/Duke	2.5	0.55–2.2

[a]With the parameters providing consistent vertical beam sizes in [23].

retaining the visibility in a reasonable range and a relatively small D_y is chosen.

To distinguish these two types of systems, we can define two figures of merit as the following:

$$g_1 = \frac{D_y}{d} \quad \text{and} \quad g_2 = \frac{2\pi D_y \sigma_y}{\lambda L_1}. \tag{22}$$

The ratio of the slit separation to the slit opening, g_1, is roughly the number of significant interference fringes inside the diffraction envelope. The second figure of merit, g_2, is the optical phase difference of the wave reaching the two slits if it is emitted at the beam height $y_e = \sigma_y$. In fact, g_2 is directly related to the visibility: $g_2 = \sqrt{-2\ln(V)}$. Using these two figures of merit, comparisons can be made between a conventional SRI system for routine synchrotron light source operation and a specially designed system for beam physics research in which the beam size varies in a wide range, such as the study of the IBS effect (see Table I). Clearly, for the conventional SRI systems, g_1 is typically large (5–15) while g_2 is small (typically less than unity) for good visibility; for the beam study that the beam size varying in a wide dynamic range, the SRI system would have a smaller g_1, but a wide range of g_2, thus visibility values.

In Table I, we also compare three SRI systems: two conventional systems (Cases 1 and 2) from KEK-ATF and BESSY II [21–23], respectively, with a new SRI system (Case 3) developed at the Duke storage ring. The design choices for g_1 and g_2 can be clearly different for these two types of systems. The detailed design parameters for our SRI system will be provided in the following section, followed by a simulation study to validate the new fitting model for this system.

B. Model validation using simulation

The new SRI system developed for the Duke storage ring can be represented using the layout shown in Fig. 2, and the designed parameters are listed in Table II. In addition to a UV filter with a central wavelength of around 340 nm and a bandwidth of 10 nm (FWHM) listed in the table, a second near-infrared filter (700 nm) can be used to extend the range of the beam size measurement. For this system, a series of simulations have been conducted with Synchrotron Radiation Workshop, a commonly used computer simulation code [24], and the resulting interference fringes on the observation plane are then analyzed and compared using the new general fitting model and the old fitting model.

TABLE II. Design and measured parameters of the newly developed SRI system at the Duke storage ring and a set of key parameters used in simulations and measurements. The central wavelength of the bandpass filter is that specified by the vendor.

Parameters	Unit	Scenario 1	Scenario 2	Measurements
L_1	m	2	2	1.96
L_2	m	2	2	1.87
λ	nm	340	340	340 ± 2 (vendor)
D_y	mm	5	5	4.86 ± 0.02
d	mm	0.2–2	2	1.70 ± 0.04
σ_y	μm	32.1	12–48	14.6–45.7
E_b	MeV	1000	1000	562

The new fitting model is compared with the old one for two scenarios: simulated beam size "measurements" (1) with a relatively large g_2 while varying g_1 and (2) with a relatively small g_1 while varying g_2. In the first scenario, a series of double slits with a fixed separation D_y and varying opening size d are used while the beam size is fixed. In the second scenario, a double slit with both fixed separation D_y and slit opening d is used while the beam size is varied in a large range. The choice of vertical electron beam size and slit parameters for these two scenarios are shown in Table II.

The simulated intensity distribution is fitted using both the old model and the new model. For the new model, an effective slit separation D_y^{eff} is obtained using Eq. (18). This effective slit separation is then used to determine the beam size via the visibility formula or Eq. (19). It should be noted that the old fitting model Eq. (20) fails for the cases with a large d and low visibility, as shown in Fig. 5. To produce reasonable fits, this model is technically modified by changing two constants c_i to two additional fitting parameters q_i ($i = 1, 2$) to produce better fitting as shown here:

$$I_1(y) = p_0 + p_1 \text{sinc}^2(q_1 y + p_2) \times \left\{1 + e^{-p_3} \cos\left[q_2\left(y + \frac{p_2}{q_1}\right)\right]\right\}. \tag{23}$$

Due to the lack of a physics interpretation in the old model, the fit value q_2 is discarded, not viewed as being related to the effective slit separation. Instead, the design value of the slit separation is used in the visibility formula.

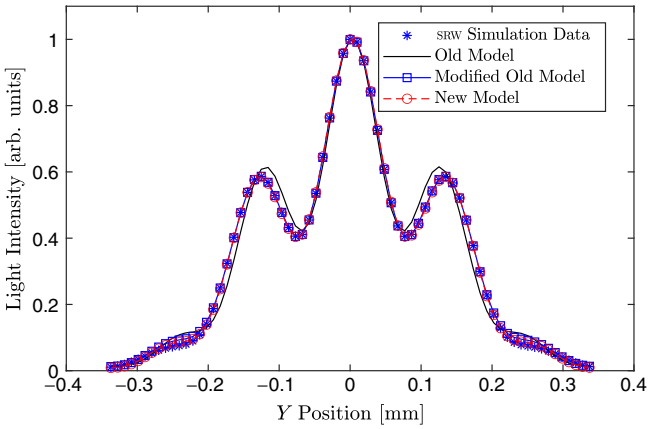

FIG. 5. Comparison of fitting simulated fringe data with three models: the old model (black line), the modified old model (blue rectangle line), and the new model (the red circle dash line). It shows that the modified old model and the new model provide reasonable fittings while the old model fails. The SRW simulation data are the simulated vertical intensity distribution of measurement using a $D = 5$ mm and $d = 2$ mm double-slit plate for a 1000 MeV beam with 32.1 μm vertical beam size.

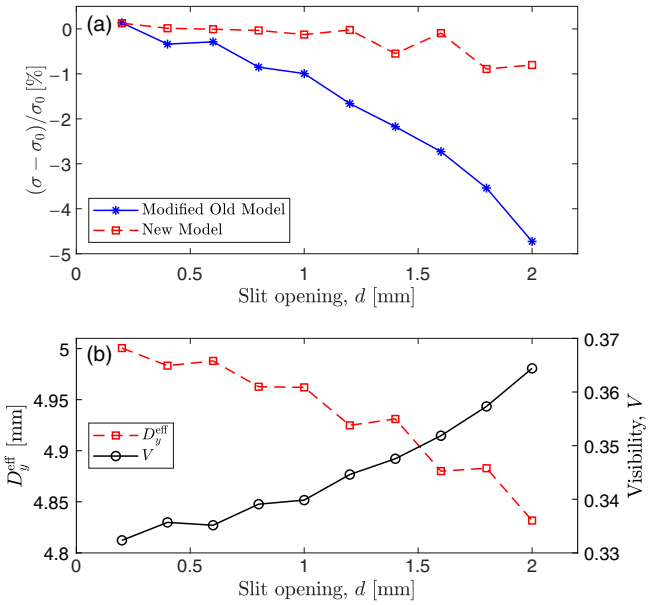

FIG. 6. Simulation results for a fixed size beam using a double slit with a fixed slit separation but a varying slit opening. (a) The relative difference between the fit beam size and the actual beam size. The blue solid line is the result using the old modified model; the red dashed line is the result based on the new model. (b) The effective slit separation D_y^{eff} and visibility V extracted from the fit parameters in the new model. The beam energy is 1000 MeV, $\sigma_y = 32.1$ μm, $D_y = 5$ mm, $L_1 = 2$ m, $L_2 = 2$ m, and a $\lambda = 340$ nm wavelength filter is used in the simulation.

When compared with the old model, the modified old model significantly improved the fitting as shown in Fig. 5, producing an acceptable overall fitting. As a result, the root-mean-square (rms) difference between the raw data and the fit using the modified old model is significantly reduced to about 20% of that with the old model. The new model further improves the fitting with this rms difference reduced to about 14% of that with the old model. Because the modified old model can produce reasonable fitting results consistently for the set of data under study, this model will be compared with the new model.

In the first set of simulations, the vertical beam size is selected to be $\sigma_0 = 32.1$ μm, so that the corresponding theoretical visibility is close to 0.33, which is considered to be the optimal condition for size measurement [14]. The simulated intensity fringes with different slit openings are fitted using the modified old model and the new model, and then the resulting beam sizes are calculated using designed separation and effective separation, respectively. This "measured" beam size is compared with the actual beam size σ_0 as shown in Fig. 6(a) with a fixed slit separation $D_y = 5$ mm while varying the slide opening d. The effective slit separation D_y^{eff} extracted from the fitting is shown in Fig. 6(b). It is observed that the results from both models agree with the designed value very well when d is very small. However, with an increasing d, the beam size extracted from the modified old model tends to be smaller than σ_0—it is about 4.7% smaller than σ_0 when d is increased to 2 mm. This would be translated to an error of about 9% in terms of the beam emittance. However, the new model provides more consistent beam size results when d varied in a wide range from 0.2 to 2 mm, with the relative beam size error of less than 1% for the entire range (or less than 2% error in terms of the beam emittance). This improved result mainly stems from the capability of the new model to precisely extract the effective separation D_y^{eff}, which is a critical parameter for the beam size calculation. The model determined D_y^{eff} is reduced as d is increased as shown in Fig. 6(b). This change is mainly responsible for the model's ability to more accurately determine the beam size. The fact that the effective separation D_y^{eff} decreases with an increasing d is consistent with the behavior predicted by the theoretical analysis of Eq. (14). It is worth noting that a related consequence is that the fit visibility is slightly increased for a large d.

With two additional parameters to produce a better fit, the modified old model does not have the insight of an effective slit separation, D_y^{eff}. However, if we artificially inject this understanding into this fitting model, we can also obtain a value for the effective slit separation D_y^{eff}, extracted from the fitting parameter q_2 [see Eq. (18)]. It can be used in the visibility formula to calculate the beam size, which results in a value closer to the designed value compared with the result calculated using D_y. However, due to the lack of the sine-like terms, this technique leads to an overcorrection of the beam size, i.e., the resulting beam size is somewhat larger than the actual value.

In the second set of simulations, the slit separation and the slit opening are fixed at 5 and 2 mm, respectively, while the beam size is varied in the range from 12.0 to 48.0 μm. Therefore, the corresponding designed visibility is changed from 0.086 to 0.857, which can be considered a large visibility range for the measurement. This range is chosen to reduce the impact on the beam size measurement due to the intensity difference of the light illuminating two slits according to [25]. The intensity distributions are fit using two models and the beam sizes are calculated separately. The resulting beam sizes are compared with the theoretical values as shown in Fig. 7(a) while the effective slit separation and the visibility extracted from the fit parameters are shown in Fig. 7(b).

It is observed that the relative difference between the beam size from the modified old model and the actual beam size σ_0 increases as the beam size is increased (or the visibility is reduced). This difference is increased to about 7.9% when $\sigma_0 = 48$ μm. The beam size obtained using the new model is more consistent with σ_0, with a relative difference of less than 1% for the entire beam size range. This stems from the new model's capability in correctly determining D_y^{eff} which decreases as σ_0 is increased as shown in Fig. 7(b). This shows that the new physics insight incorporated into the new model is very important for the accurate measurement of a large beam with small visibility.

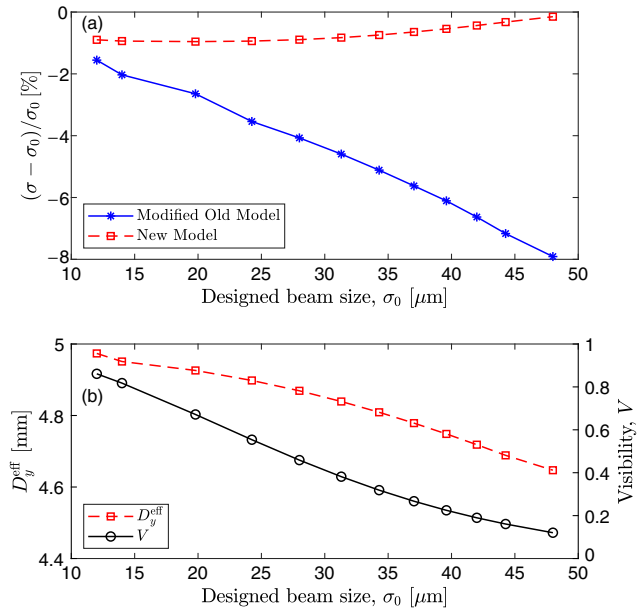

FIG. 7. Simulation results using a double slit with a fixed slit separation and a fixed slit opening for beams with varying sizes. (a) The relative difference between the fit beam size and the actual beam size. The blue solid line is the result of the old modified model and the red dashed line is the result of the new model. (b) The effective separation D_y^{eff} and the visibility V extracted from the fit parameters using the new model. The beam energy is 1000 MeV, $D_y = 5$ mm, $d = 2$ mm, $L_1 = 2$ m, $L_2 = 2$ m, and a 340-nm wavelength filter is used in the simulation.

This is especially important when a double slit with a relatively small $g_1 = D_y/d$ is used. This behavior confirms the insight revealed in Eq. (16) that the importance of the sine-like term in the diffraction envelope is increased for a reduced g_1.

In this section, two sets of simulations are presented to show the robustness of the new model in finding the beam size with high accuracy in two scenarios: (1) measuring a beam using a double slit with a fixed D_y but a varying d, i.e., a varying $g_1 = D_y/d$; (2) using a double slit with a small g_1 to measure the beams of different sizes or a varying g_2. The simulation results have confirmed that the new model is capable of producing consistent and accurate beam size results in both scenarios. Specifically, in the case that g_1 is relatively small so that there are a few interference fringes inside the main diffraction envelope, the new model provides a more reliable fitting compared with the conventional model (the modified old model). With a large slit opening so that $g_1 = 2.5$, the new model provides reliable results in a wide range of measured visibility from 0.120 to 0.861 (computed using D_y^{eff}). In this wide range of visibility, the beam size is determined with a relative error of less than 1% using the new model.

V. APPLICATION AT DUKE STORAGE RING

At the Duke storage ring, we have developed an SRI system for the vertical beam size measurement for routine operation from 250 MeV to 1.2 GeV and for the beam study with the beam size/current varying in a wide range. This system is designed to be capable of (1) measuring the electron beam size at an ultralow current; and (2) measuring the beam with its size varying in a wide range. The first requirement is met by using a double slit with a large slit opening d to allow sufficient light to pass through. The second requirement is met by developing an SRI with a wide dynamic range, i.e., capable of performing accurate measurements with both low and high visibility. The key design parameters for our system are shown in Table II, with similar values for the simulated SRI in the previous section. The slit is made using a 3D printer with an opening $d = 1.70$ mm and a slit separation $D_y = 4.86$ mm (both measured values), resulting in a small $g_1 \approx 2.86$. By using the new fitting model, we expect that this system can work with a wide range of visibility, $V = 0.2$ to 0.8 for accurate measurements. Using a UV filter with the central wavelength $\lambda_0 = 340$ nm, the designed range of the beam size measurement is from 14.6 to 39.2 μm, a factor of 2.7. In the following, we will present experimental results from two types of measurements: (1) low beam current measurements ($I \approx 0.01$ mA) and (2) measurements at a higher current ($I \approx 10$ mA) with a varying beam size.

Figure 8 shows the measurement of an electron beam with a very low current. A total of 22 beam images are taken with the same exposure time (1s) and the same gain.

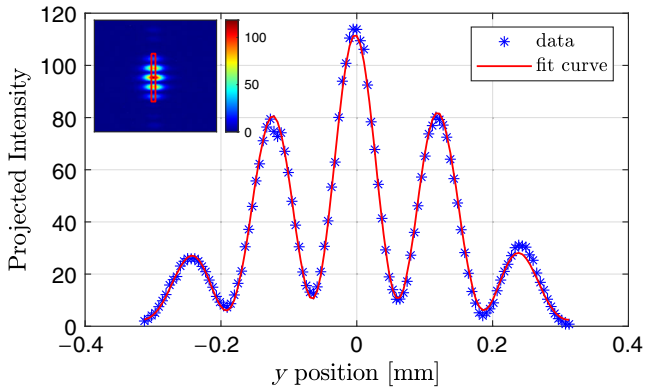

FIG. 8. Beam size measurement for a low current beam at the Duke storage ring. The main plot shows the projected vertical intensity distribution of the image. The blue stars are the average value of the image intensity in the selected area shown as a red rectangle in the inserted image and the red solid line is the fit curve using Eq. (17). The inset shows the average image of 22 images taken using a CMOS camera with the same exposure time (1s) and a constant gain with the background subtracted. The beam current is determined to be 12.5 ± 0.2 μA using an imaging technique, and the beam size is measured to be 14.6 ± 0.4 μm. The storage ring is operated at 562 MeV in a multibunch mode

The average of all these images, shown as an inset of Fig. 8, is used for the fitting and analysis. The projection of the averaged image in the selected area (the red rectangle region in the inset) is used for fitting with the new model. The interference pattern and the related fit are shown in the main plot of Fig. 8. Based on the fitting, the beam size is calculated using Eq. (19), $\sigma_y = 14.6 \pm 0.4$ μm, with a visibility of 0.817. The beam current is determined using a technique based on the integrated image intensity [26], which results in a measured beam current $I_e = 12.5 \pm 0.2$ μA, a very low current for the storage ring operation.

The second set of measurements is conducted with the same double slit for a range of beam sizes. The vertical beam size increase is realized by reducing the vertical and horizontal betatron tune difference to increase the transverse emittance coupling of the storage ring lattice. During the measurement, the electron beam current is kept at about 10 mA, a much higher current compared to the first set of measurements in order to reduce the exposure time for the camera. The measurements are made using a fixed exposure time (20.5 ms) to produce an image with reasonable pixel values. For each emittance coupling setting, ten images are taken to determine the measurement uncertainty. The measurement results are shown in Fig. 9.

It is observed in Fig. 9(a) that the depth of the valleys in the interference pattern is reduced with the increase of emittance coupling among eight sets of measurements, S_1 to S_8. The measured visibility decreased from 0.547 to 0.154 [see Fig. 9(c)]. The measured beam size is found to increase from 24.3 to 45.7 μm as shown in Fig. 9(b), with the relative measurement uncertainty (statistical) changing

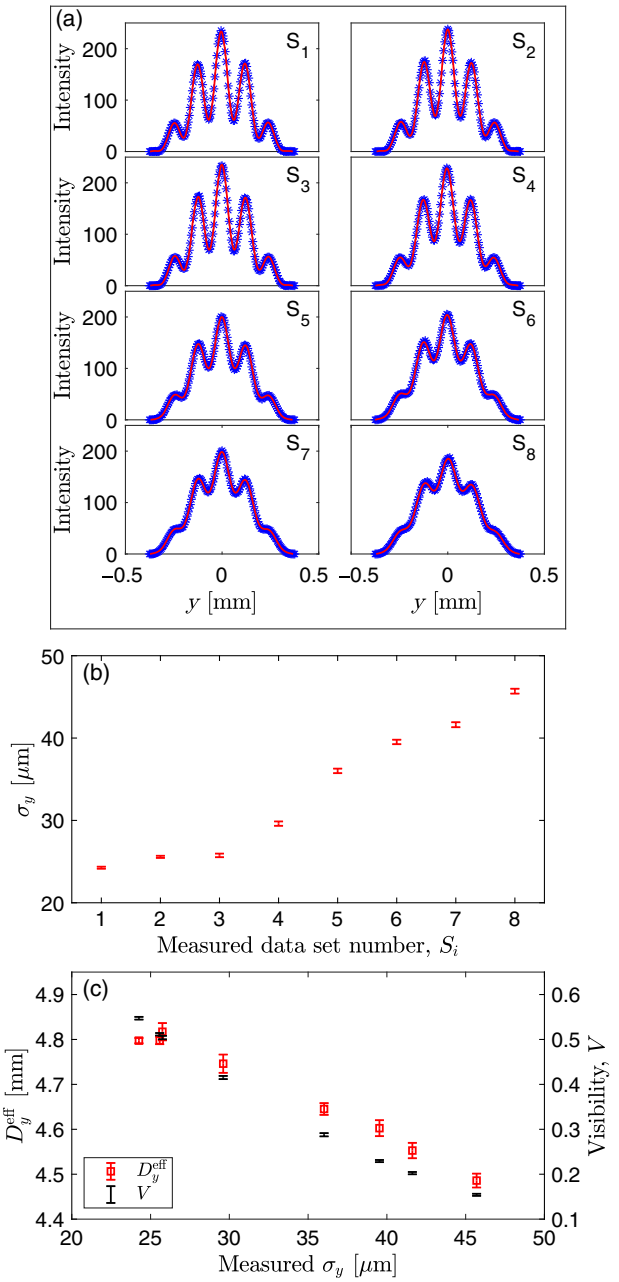

FIG. 9. Beam size measurements with a varying vertical size using setups of the storage ring lattices with different emittance coupling. (a) For each of the eight sets of measurements, a representative intensity distribution (blue stars) and fitting curve (red lines) are shown, selected from one of the ten images. (b) The measured beam size with the statistical error based on ten images for each set of measurements. (c) The effective slit separation and measured visibility versus the measured beam size. All the measurements are performed with a single beam operated at 562 MeV with a current of about 10 mA.

from 0.5% to 0.9%. Figure 9(c) shows that the D_y^{eff} decreases with the increase of the measured beam size σ_y, a trend explained in Fig. 7(b). The relative reduction of D_y^{eff} is 6.9% among the eight measurements, which is

also in qualitative agreement with the simulation result, a reduction of 4.4% [in Fig. 7(b)] for the same range of the visibility reduction.

These two types of measurements with very different beam currents and emittance coupling settings have shown that our SRI system is also capable of measuring the vertical beam size in a wide dynamic range from 14.6 to 45.7 μm, a factor of 3.13. This corresponds to a large range of visibility from 0.154 to 0.817.

VI. SUMMARY AND DISCUSSION

The development of an SRI-based beam size measurement system for various beam studies, including the IBS study, faces two major challenges: (1) measuring the beam size at an ultralow current and (2) measuring the beam size in a wide dynamic range, including large beams with a low visibility. To meet the first challenge, a double slit with a large slit opening d can be used to allow for sufficient light onto the camera sensor. In the meantime, the choice of the slit separation (D_y) is limited by the need to have the double slit illuminated by the core part of synchrotron radiation with higher intensity. Therefore, such a system requires a relatively small $g_1 = D_y/d$, compared with conventional SRI systems developed for routine operation of storage ring–based light sources. The conventional SRI uses a physics model (the old model) that approximates synchrotron radiation with a uniform amplitude spherical wave and assumes a reasonably large visibility in a small dynamic range. These assumptions are problematic for an SRI system for the IBS study due to the use of a large slit opening and the need for a large dynamic range.

To extend the SRI method for a wider range of applications, we have analyzed the impact of the nonuniform wave amplitude and the impact of the varying visibility (due to a changing beam size) on the beam size measurement. Our analysis has revealed that: (1) the effective slit separation is reduced with the increase of the slit opening; and (2) a sine-like term is necessary to be included to describe the diffraction envelope in a more general form. These findings are particularly important for the cases when both the slit opening d and the beam size σ_0 are large (i.e., at a low visibility). In this work, we have proposed a new general model for the SRI method with several additional fitting parameters. This new model allows us to determine an effective slit separation D_y^{eff}, which is used for the beam size calculation. This new model has been validated using the simulation results. In Sec. IV, we have shown that the new model is robust in two important areas: (1) it provides consistent and accurate beam size results for a range of choices of the slit opening; and (2) it provides accurate results for a wide range of beam sizes, i.e., a change of the beam size by a factor of 4 (see the simulation results in Sec. IV), using a double slit with a large slit opening. Therefore, the new model developed in this work is well suited for beam size measurements at a low beam current and with a wide range of beam sizes.

We have developed an SRI system dedicated for the intrabeam scattering study on the Duke storage ring. This system uses a double slit with a relatively large slit opening $d = 1.7$ mm and a relatively small $g_1 = 2.86$. This system has been used to measure a small vertical beam size, 14.6 ± 0.4 μm, at a low current beam (12.5 ± 0.2 μA). It has also been used to measure the changing vertical beam size by increasing the emittance coupling in the storage ring with the beam size varying from 24.3 to 45.7 μm or in the range of measured visibility from 0.154 to 0.547. More details about the design, calibration, and practical considerations of Duke's SRI system will be presented elsewhere in a separate publication.

Motivated by the need to develop an instrument for the intrabeam scattering research, the new model presented in this work has significantly extended the applicable range of the SRI techniques for the beam size measurement. This new model can have other important applications. First, because of the additional built-in physics insights, the new model can be used for the existing conventional SRI systems to improve the measurement accuracy by reducing the systematic errors associated with the less capable old model, especially for those employing a double slit with a large slit opening or when used to conduct measurements at a low visibility due to a large size beam. Second, the low beam current capability can be further explored by combining a large slit opening with a high-sensitivity camera with active cooling and by optimizing the operational wavelength for the system. The ultralow light capability is available for a direct image-based system: it has been reported that such a system can measure the transverse profile of a 50-pC electron beam in a single pass [27]. Therefore, it will be interesting to explore the possibility of using an SRI system to measure a single-pass electron beam, for example, as a nondestructive optical diagnostic for an energy-recovery linac or a single-pass free-electron laser.

ACKNOWLEDGMENTS

The experimental research was carried out using the accelerator at the High Intensity Gamma-ray Source (HIGS) facility at Triangle Universities Nuclear Laboratory (TUNL). We would like to thank the engineering and technical staff at HIGS/TUNL for their support. This work is partially supported by DOE Grant No. DE-FG02-97ER41033.

APPENDIX A: IMPACT OF NONUNIFORM WAVE AMPLITUDE

For synchrotron radiation, the nonuniform wave amplitude of the σ-polarized component can be described in terms of a power series on the double-slit plane,

$$A(\theta) = a_0(\theta_0) + \sum_{n=1}^{+\infty} a_i(\theta_0)|\theta - \theta_0|^i, \tag{A1}$$

where $a_0(\theta_0)$ is the wave amplitude at an observation angle θ_0. Let us simplify our discussion by keeping only the two lowest order terms, and the effect of higher-order terms can be treated similarly.

First of all, let us focus on the upper slit with $\theta_0 = D_y/(2L_1)$, such that

$$A(\theta) \approx a_0 + a_1 \frac{y_s - D_y/2}{L_1} = a_0[1 - \alpha \Delta y_s], \tag{A2}$$

where $\alpha = -a_1/(a_0 L_1) > 0$, $\Delta y_s = y_s - D_y/2$, $a_0 = a_0(\theta_0)$, and $a_1 = a_1(\theta_0)$. Assuming that the change of the wave amplitude is small, we have $|\alpha \Delta y_s| \ll 1$. As a result, Eq. (2) can be written as

$$\begin{aligned} U_1(y_e, y) &= \frac{ik}{2\pi} \int_{S_1} \frac{a_0(1 - \alpha \Delta y_s)}{R_1 R_2} e^{[-ik(R_1 - \frac{y_s^2}{2f} + R_2)]} dS, \\ &\propto \int_{S_1} (1 - \alpha \Delta y_s) e^{i\beta \Delta y_s} e^{i\beta \frac{D_y}{2}} dy_s, \end{aligned} \tag{A3}$$

where $\beta = k(\frac{y_e}{L_1} + \frac{y}{L_2})$. The integration over the upper slit S_1 can be performed as follows:

$$\begin{aligned} &\int_{S_1 - \frac{D_y}{2}} (1 - \alpha \Delta y_s) e^{i\beta \Delta y_s} e^{i\beta \frac{D_y}{2}} d\Delta y_s \\ &\quad = e^{i\beta \frac{D_y}{2}} d \left\{ \sin c\left(\frac{\beta d}{2}\right) - i \frac{\alpha}{\beta} \left[\sin c\left(\frac{\beta d}{2}\right) - \cos\left(\frac{\beta d}{2}\right) \right] \right\}. \end{aligned} \tag{A4}$$

The lower slit can be treated similarly, by replacing $D_y/2$ with $-D_y/2$, and replacing α with $-\alpha$. Consequently, the electric field passing through the double slit on the observation plane can be obtained as

$$\begin{aligned} U(y_e, y) &\propto \operatorname{sinc}\left(\frac{\beta d}{2}\right) \left\{ \cos\left(\frac{\beta D_y}{2}\right) \right. \\ &\quad \left. + \frac{\alpha}{\beta} \left[1 - \cot\left(\frac{\beta d}{2}\right) \frac{\beta d}{2} \right] \sin\left(\frac{\beta D_y}{2}\right) \right\} \\ &\approx \operatorname{sinc}\left(\frac{\beta d}{2}\right) B \cos\left(\frac{\beta D_y}{2} + \chi\right), \end{aligned} \tag{A5}$$

where $\tan(\chi) = -(\frac{\alpha\beta d^2}{12} + \frac{\alpha\beta^3 d^4}{720})$ and $B = \sqrt{1 + (\frac{\alpha\beta d^2}{12} + \frac{\alpha\beta^3 d^4}{720})^2}$. An approximation of $\cot(\frac{\beta d}{2}) \approx \frac{2}{\beta d} - \frac{1}{3}\frac{\beta d}{2} - \frac{1}{45}(\frac{\beta d}{2})^3$ is used with a reasonable assumption of $\frac{\beta d}{2} \ll \pi$.

For a uniform wave amplitude where $\alpha = 0$, Eq. (A5) is reduced to the conventional expression of Eq. (5). Let's assume a small α and a small d, which leads to a small χ ($|\chi| \ll 1$). As a result, we have $\chi \approx -(\frac{\alpha\beta d^2}{12} + \frac{\alpha\beta^3 d^4}{720})$, and the intensity on the observation plane can be obtained for a single electron

$$\begin{aligned} \frac{I(y_e, y)}{I_0} &\propto \operatorname{sinc}^2\left(\frac{\beta d}{2}\right) B^2 \cos^2\left(\frac{\beta D_y}{2} + \chi\right) \\ &\approx \operatorname{sinc}^2\left(\frac{\beta d}{2}\right) B^2 \cos^2\left(\frac{\beta D_y^{\text{eff}}}{2}\right), \end{aligned} \tag{A6}$$

with

$$D_y^{\text{eff}} = D_y - \frac{\alpha}{6} d^2 \left[1 + \frac{\pi^2}{15} \left(\frac{\beta d}{2\pi}\right)^2 \right]. \tag{A7}$$

When the slit opening d is very small, i.e., $\beta d \ll 2\pi$, the higher-order term can be ignored and it can be simplified as

$$D_y^{\text{eff}} = D_y - \frac{\alpha}{6} d^2. \tag{A8}$$

It can be observed that $D_y^{\text{eff}}/D_y < 1$ when $\alpha > 0$ as in the case of synchrotron radiation which peaked in the forward direction with $\theta = 0$. Therefore, we expect the effective slit separation D_y^{eff} to be smaller than the design value D_y. Based on this leading order analysis, the discrepancy between these two values will increase with an increased slit opening d and amplitude gradient α. The expression of Eq. (A7) also shows some dependency of D_y^{eff} on the beam size σ_0 (according to y_e in β). It can be expected that the effective slit separation would decrease as the beam size is increased for a double slit with a fixed opening.

APPENDIX B: IMPACT OF BEAM SIZE

The diffraction term $\operatorname{sinc}^2\psi(y_e, y)$ in Eq. (10) can be expanded as a function of y_e around the electron beam center y_0, the first-order expansion can be written as follows:

$$\operatorname{sinc}^2\psi(y_e, y) = \operatorname{sinc}^2\psi_0(y) + C[\psi(y_e, y) - \psi_0(y)], \tag{B1}$$

where

$$\begin{aligned} C &= 2\operatorname{sinc}^2\psi_0(y) \left[\frac{\cos\psi_0(y)}{\sin\psi_0(y)} - \frac{1}{\psi_0(y)} \right] \\ &\approx \operatorname{sinc}^2\psi_0(y) \left[-\frac{2\psi_0(y)}{3} \right]. \end{aligned} \tag{B2}$$

To simplify the expression, let us denote $Y = y_e - y_0$ and $Y' = \frac{y_0}{L_1} + \frac{y}{L_2}$. As a result, the integration of the first-order term can be written as

$$\begin{aligned}\frac{I_1(y)}{I_0} &= \int_{-\infty}^{\infty} C\frac{\pi d}{\lambda L_1} Y\left[1+\cos\left(\frac{2\pi D_y}{\lambda L_1}Y+\frac{2\pi D_y}{\lambda}Y'\right)\right]\rho(Y)dY \\ &= \int_{-\infty}^{\infty} C\frac{\pi d}{\lambda L_1} Y\left[1+\cos\left(\frac{2\pi D_y}{\lambda L_1}Y\right)\cos\left(\frac{2\pi D_y}{\lambda}Y'\right)\right. \\ &\quad \left.-\sin\left(\frac{2\pi D_y}{\lambda L_1}Y\right)\sin\left(\frac{2\pi D_y}{\lambda}Y'\right)\right]\rho(Y)dY \\ &= -\int_{-\infty}^{\infty} C\frac{\pi d}{\lambda L_1} Y\sin\left(\frac{2\pi D_y}{\lambda L_1}Y\right)\sin\left(\frac{2\pi D_y}{\lambda}Y'\right)\rho(Y)dY. \end{aligned} \tag{B3}$$

In the last step, we use the assumption that the charge density distribution $\rho(Y)$ is an even function of Y.

For a Gaussian beam distribution in the vertical direction, the above equation can be integrated,

$$\begin{aligned}\frac{I_1(y)}{I_0} &= -C\frac{1}{2}\left(\frac{2\pi D_y}{\lambda L_1}\sigma_y\right)^2\frac{d}{D_y}\exp\left[-\frac{1}{2}\left(\frac{2\pi D_y}{\lambda L_1}\sigma_y\right)^2\right] \\ &\quad\times\sin\left(\frac{2\pi D_y}{\lambda}Y'\right) \\ &= -C\ln\left(\frac{1}{V}\right)\frac{d}{D_y}V\sin\left[\frac{2\pi D_y}{\lambda}\left(\frac{y_e}{L_1}+\frac{y}{L_2}\right)\right], \end{aligned} \tag{B4}$$

where V is the visibility as defined in Eq. (11).

This calculation can be carried out by expanding the diffraction term to the higher orders. It can be found that the expansion to the odd-order terms results in a sine-like term and the expansion to the even-order terms results in a cosine-like term. Therefore, it is important to have both sine- and cosine-like terms in the fitting model.

[1] G. Kube, in *Proceedings of the 8th European Workshop on Beam Diagnostics and Instrumentation for Particle Accelerators, DIPAC 2007, Venice, Italy* (JACoW, Geneva, Switzerland, 2008), pp. 6–10.

[2] S. Takano, M. Masaki, and H. Ohkuma, in *Proceedings of the 7th European Workshop on Beam Diagnostics and Instrumentation for Particle Accelerators, DIPAC 2005, Lyons, France* (JACoW, Geneva, Switzerland, 2005), pp. 241–243.

[3] B. Yang, J. Morgan, S. Lee, and H. Shang, in *Proceedings of International Beam Instrumentation Conference, IBIC 2016, Barcelona, Spain* (JACoW, Geneva, Switzerland, 2016), pp. 504–507.

[4] S. Takano, M. Masaki, and H. Ohkuma, Nucl. Instrum. Methods Phys. Res., Sect. A **556**, 357 (2006).

[5] P. Elleaume, C. Fortgang, C. Penel, and E. Tarazona, J. Synchrotron Radiat. **2**, 209 (1995).

[6] C. Thomas, G. Rehm, I. Martin, and R. Bartolini, Phys. Rev. ST Accel. Beams **13**, 022805 (2010).

[7] Å. Andersson and J. Tagger, Nucl. Instrum. Methods Phys. Res., Sect. A **364**, 4 (1995).

[8] T. Mitsuhashi and M. Katoh, in *Proceedings of the 5th European Particle Accelerator Conference, EPAC 1996, Sitges, Spain* (JACoW, Geneva, Switzerland, 1996).

[9] M. Sjöström, H. Tarawneh, and E. Wallén, in *Proceedings of the 10th European Particle Accelerator Conference, Edinburgh, Scotland, 2006* (EPS-AG, Edinburgh, Scotland, 2006), pp. 26–30.

[10] B. Li, H. Hao, J.-y. Li, and Y. K. Wu, Nucl. Instrum. Methods Phys. Res., Sect. A **911**, 45 (2018).

[11] T. Mitsuhashi, *Beam Measurement* (World Scientific, Singapore, 1999), pp. 399–427.

[12] T. Naito and T. Mitsuhashi, Phys. Rev. ST Accel. Beams **9**, 122802 (2006).

[13] M. Born and E. Wolf, *Principles of Optics: Electromagnetic Theory of Propagation, Interference and Diffraction of Light*, 7th ed. (Cambridge University Press, Cambridge, England, 1999).

[14] M. Masaki and S. Takano, J. Synchrotron Radiat. **10**, 295 (2003).

[15] K. Tang, B.-G. Sun, Y.-L. Yang, P. Lu, L.-L. Tang, F.-F. Wu, C.-C. Cheng, J.-J. Zheng, and H. Li, Chin. Phys. C **40**, 097002 (2016).

[16] S. Wang, D. Rubin, J. Conway, M. Palmer, D. Hartill, R. Campbell, and R. Holtzapple, Nucl. Instrum. Methods Phys. Res., Sect. A **703**, 80 (2013).

[17] L. Torino, U. Iriso *et al.*, in *Proceedings of the 5th International Beam Instrumentation Conference, IBIC2016, Barcelona, Spain* (JACoW, Geneva, Switzerland, 2016).

[18] K. D. Moller, *OPTICS Learning by Computing, with Examples Using Mathcad, Matlab®, Mathematica®, and Maple®: With 308 Illustrations*, 2nd ed. (Springer, New York, 2007).

[19] A. Hofmann, *The Physics of Synchrotron Radiation*, Vol. 20 (Cambridge University Press, Cambridge, England, 2004).

[20] W. Li, J. Yan, P. Liu, and Y. K. Wu, in *Proceedings of 12th International Particle Accelerator Conference, IPAC-2021, Campinas, SP, Brazil* (JACoW, Geneva, Switzerland, 2021), pp. 3949–3952.

[21] T. Naito, T. Mitsuhashi *et al.*, in *Proceedings of the International Particle Accelerator Conference, Kyoto, Japan* (ICR, Kyoto, 2010), p. 972.

[22] H. Hayano, K. Kubo, T. Mitsuhashi, T. Naito, N. Terunuma, N. Toge, J. Urakawa, T. Okugi, and S. Kashiwagi, in *Proceedings of the 18th Particle Accelerator Conference, New York, 1999* (IEEE, New York, 1999), Vol. 3, pp. 2143–2145.

[23] M. Koopmans, P. Goslawski, J.-G. Hwang, A. Jankowiak, M. Ries, A. Schälicke, G. Schiwietz *et al.*, in *Proceedings of the 9th International Particle Accelerator Conference, IPAC-2018, Vancouver, Canada* (JACoW, Geneva, Switzerland, 2018), pp. 2103–2106.

[24] O. Chubar, P. Elleaume, S. Kuznetsov, and A. A. Snigirev, *Optical Design and Analysis Software II* (International Society for Optics and Photonics, Bellingham, USA, 2002), Vol. 4769, pp. 145–151.

[25] A. D. Garg, M. Modi, and T. Puntambekar, Nucl. Instrum. Methods Phys. Res., Sect. A **902**, 164 (2018).

[26] B. Li, Experimental study of intrabeam scattering effect in Duke storage ring, Ph.D. thesis, University of Science and Technology of China, 2018.

[27] B. Scheidt, in *Proceedings of the 7th European Workshop on Beam Diagnostics and Instrumentation for Particle Accelerators, DIPAC 2005, Lyons, France* (JACoW, Geneva, Switzerland, 2005), pp. 26–28.